Robotica (1997) volume 15, pp 483–491. Printed in the United Kingdom © 1997 Cambridge University Press

# Ultrasonic classification and location of 3D room features using maximum likelihood estimation – Part I*

Hong Mun-Li† and Lindsay Kleeman‡

*(Received in Final Form: January 8, 1997)*

**SUMMARY**

Current mobile robot ultrasonic localisation techniques use sensor systems which rely on features in a horizontal plane. The implicit assumption is that the room boundary on the horizontal plane is not obstructed by objects such as furniture. This assumption is often not realistic and restricts the versatility and portability of these systems. The solution proposed in this paper is the provision of sensing flexibility to use other 3D room boundaries (e.g. ceiling-wall intersections) as 3D natural beacons. We propose a 3D ultrasonic sensor array that uses a Maximum Likelihood Estimator to match the echo arrival times to different object classes and to determine the location of the 3D target. This method does not require fast data acquisition or powerful computing. It has been implemented on a robot localisation application with the Extended Kalman Filter. This paper is the first of two parts, and presents theoretical results on target classification and minimum transducer requirements. The second part, in the next issue of *Robotica,* presents experimental results on the characterisation of the sensor and its application to robot localisation, and includes the references for the both papers.

KEYWORDS: Ultrasonic sensors; 3D room features; Localisation; Maximum likelihood estimation.

## 1. INTRODUCTION

Ultrasonic sensors have been commonly used for the detection of obstacles in the path of the mobile robots. However, with more understanding of the physics of echolocation, considerable research has been conducted in extracting more information from the ultrasonic echoes rather than just arrival times from single transducers. As a result, ultrasonic sensing is now playing a significant role in the estimation of robot position and orientation, known as localisation.

Robot localisation methods can be broadly categorised into two groups: *dead reckoning* and *external/environmental referencing.* Dead reckoning is usually performed by odometry, which involves the integration of wheel rotation increments over time to estimate the position of a vehicle. Slippage and deformation of wheels and uneven floor surfaces inevitably accumulate increasing errors in the odometry localisation.

The odometry errors can be corrected if there are regular, independent position fixes. This can be achieved by providing the robot with the ability to reference its position with respect to external features. *Sonar maps* and *beacons* are two common types of external references used in ultrasonic robot localisation. Fusion of the external referencing information with the internal odometry data is often performed using estimation techniques such as the Kalman filter.

A sonar map of the immediate vicinity of the robot is obtained by scanning the surroundings with a rotating rangefinder[1] or a ring of rangefinders.[2,3] This sonar map of the immediate area around the robot is used as a reference.

Beacons can be further categorised into *active* and *passive.* The ultrasonic active beacons used in robot localisation are often ultrasonic transmitters that are either placed strategically in a room or carried on a mobile robot. Triangulation is a common method of referencing with active beacons. The principle is similar to the use of lighthouses in marine navigation. Kleeman[4] uses six transmitters as active beacons placed around the edges of the environment and eight ultrasonic receivers arranged in an octagon on the robot. The position and orientation of the robot can be successfully determined using the differences between the echo times of flight from three beacons. This active beacon technique has been extended to 3D localisation.[5,6] In a different approach, LeMay and Lamancusa[7] develop a 3D position measuring system which requires at least four receivers at known and fixed coordinates in a global reference frame. The aim of their system is to determine the location of a transmitter (the active beacon) in 3D space based on the arrival time of the ultrasonic pulse at each receiver. These transducers placed in the environment need to be maintained and powered.

On the contrary, ultrasonic passive beacons do not require external power. They are usually naturally occurring features in the environment which serve as acoustic positional references for the robot. Most such beacons used in an indoor environment are walls (planes), 2D corners, 2D edges and cylinders (table legs).

* This work was conducted at the Dept. of Electrical and Computer Systems Engineering, Monash University, Clayton, Australia and was supported by a Monash Graduate Scholarship.

† School of Applied Science, Nanyang Technological University (Singapore).

‡ Intelligent Robotics Research Centre, Department of Electrical and Computer Systems Engineering, Monash University, Clayton, Victoria 3168 (Australia.)

https://doi.org/10.1017/S0263574797000581 Published online by Cambridge University Press

Sabatini,[8] Peremans et al.,[9] Kleeman et al.[10] and Ko et al.[11] all use time of flight measurements in the identification algorithms, while Kuc et al.[12,13] use *echo amplitudes* to achieve object identification. Sasaki et al.[14] classifies objects based on the phase and gain Bode plots of an acoustic transfer function.

However, these sensing strategies work in 2D space. The sensors invariably scan for walls and wall-wall intersections in a horizontal plane. The implicit assumption is that the room boundary in the scanning plane is not obstructed by objects such as furniture. This problem may be avoided if the sensor system has the *flexibility* to track some other room boundaries, such as the ceiling-wall intersections when the need arises. The system must then be able to *classify and locate in 3D space* common room features or landmarks such as (1) walls (planes), (2) wall-wall, ceiling-wall or floor-wall concave corners (2D corners) and (3) concave corners formed by two walls and the ceiling or floor (3D corners).

The aim of the research presented in this paper is the design of a simple yet robust sensing strategy for robot localisation in an indoor environment. The sensing strategy described here exploits the unique relationship between the nine echo arrival derived from three ultrasonic transceivers. The Maximum Likelihood Estimator (MLE) is used to classify the object under observation and to obtain the most likely location of the identified reflector.

This method has several advantages. Firstly, it requires only *one* sensor observation cycle to perform target classification and localisation. A sensor is defined in this work as a measuring *system* consisting of one or more transducers and the necessary software and hardware support, while a transducer is a single energy-converting device.

Secondly, neither a fast data acquisition system nor a powerful computer is required, thus achieving the practical considerations of design simplicity and cost effectiveness. The algorithm has been implemented on a low sampling rate (59 kHz) sensor system using simple linearisation of the rising envelope edge of echo signals to measure echo arrival times.

Thirdly, it can classify and locate true 3D natural beacons in 3D space. Using the convention shown in Figure I-1 where the sensor lies on the *uv* plane, the object distance, *R*, is measured along the normal of the plane, the normal to the concave edge in a 2D corner, or from the vertex of the 3D corner. This is an improvement on many ultrasonic sensing systems which can only localise reflectors on a 2D surface such as the *vw* plane. There are other 3D target localisation and classification techniques.[15,16] By comparison, the 3D sensing strategy developed in this research is simpler in hardware and processing, faster and cheaper. However, accuracy and maximum range are sacrificed to some degree.

Some earlier results of this work have been summarised.[17] The first part of this paper describes previously unpublished derivations of object classification and important theoretical results on the minimum transducer requirements for 3D target classification. The derivations of object location, the experimental resuts on 3D object classification and location, and the results collected from applying the sensor system to robot localisation will be published in the next issue of Robotica. Figures, tables and equations have the prefix I or II to indicate which part they are located.

## 2. MINIMUM NUMBER OF TRANSDUCERS

Since the wavelength of the ultrasound employed in the sensor is long (about 7 mm at a frequency of 50 kHz) compared to surface features, reflections off smooth objects such as plaster walls can be considered specular and the angle of incidence is equal to the angle of reflection. A transmitter can therefore be replaced by its *virtual image* without losing any integrity of information. This is useful in illustrating the signal paths during multiple reflections.

Figure I-2 shows the positions and orientations of a transducer and its virtual image when the reflector is a plane and a 2D corner. In both cases, the virtual image and the transducer are equidistant from the point of reflection. The echo arrival times measured would be equal and no information on the reflector type can be obtained.

Introduction of a second transducer into the sensor system resolves the ambiguity between a plane and 2D corner shown in Figure I-2. The two transducers operate as two transmitters and two receivers. When one transducer transmits, both transducers will receive the resulting echoes. The time of flights measured are

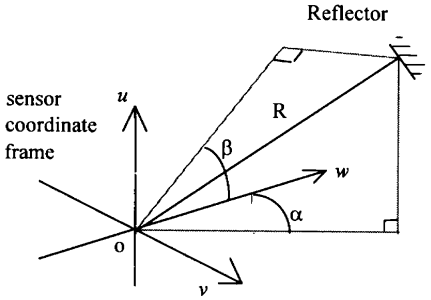


Fig. I-1. Position and orientation of reflector with respect to sensor frame.

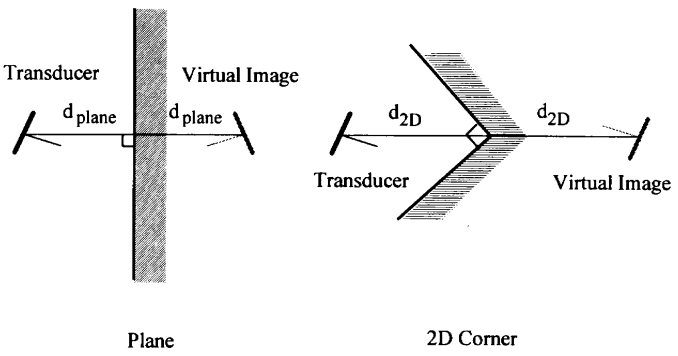


Fig. I-2. A transducer and its virtual image in reflections off a plane and a 2D corner.

https://doi.org/10.1017/S0263574797000581 Published online by Cambridge University Press

proportional to the distances between the transducers and their virtual images (e.g. $T1–T1'$, $T1–T2'$) in Figure I-3. Even when $d_{\text{plane 1}}$, $d_{\text{plane 2}}$, $d_{2D1}$ and $d_{2D2}$ are all equal, the virtual images are at different positions with respect to the transducers (Figure I-3). The resulting differences in the time of flights measured between cross transducers will be the differentiating criteria between a plane and a 2D corner.

When the reflector is a 3D corner, the corresponding virtual images of this two-transducer sensor lies in the opposite quadrant about the 3D corner vertex. As a result, the positions of these virtual images will not be different from those when the same sensor is suitably placed over a 2D corner as illustrated in Figure I-4.

In Figure I-5, the virtual images of three coplanar but non-collinear transducers and their virtual images are shown for the cases when the reflector is a plane and when it is a 3D corner. When the reflector is a plane, the virtual images are mirror images of the transducers, and the reflection paths $T1–T1'$, $T2–T2'$ and $T3–T3'$ are parallel to each other. However, when the reflector is a 3D corner, all three reflection paths intersects at the vertex of the corner. The positions of the virtual images are thus different in these two cases.

In Figure I-6, projections parallel and perpendicular to the concave edge are used to illustrate the case of a 2D corner reflector. The reflection paths intersect at the concave edge in the top projection and are parallel in the side projection. Unique virtual images for reflections off one, two and three orthogonal surfaces are thus produced with the inclusion of a third non-collinear transducer. Planes, 2D and 3D corners can therefore be distinguished by *three* or more transducers.

## 3. SENSOR CONFIGURATION

A minimum of three non-collinear transducers are necessary to distinguish between a 3D corner and a 2D corner. Our sensor system consists of three transducers arranged at the vertices of an equilateral triangle with sides of length $d$. These transducers are transceivers, operating as both acoustic transmitters and receivers. The sensor coordinate frame is defined in Figure I-7. The $w$ axis is perpendicular to the sensor plane and points in the same direction as the transducers. The $v$ axis is parallel to the line joining transducers 1 and 2, and the origin of the coordinate frame, $o$, is at the centre of the triangular structure.

The three transducers transmit in turn. After each transmission, all transducers enter into receiving mode for a fixed period of time before the next transducer transmits a pulse. This transmission-reception pattern gives a set of nine received echoes per sensor cycle.

## 4. DEGREES OF FREEDOM (DOF)

*(a) The 3D reflectors or beacons*

Table I-1 shows the 3D representation recognised by the sensor system and the degrees of freedom (DOF) for the planes, 2D and 3D corners. A plane is minimally defined by three parameters and therefore has three DOF. The positions of the virtual images for a 3D corner reflector are only dependent on the position of the vertex of the corner which is a point in space. A 3D corner therefore also has three DOF. The positions of the virtual images over a 2D corner are dependent only on the relative position of the transducers with respect to the concave edge of the corner and not the corner's orientation about that edge. As a result, 2D corner is defined by a line in 3D space which has four DOF (three DOF for a plane in which the line lies and another for the angle of the line in that plane).

*(b) The sensor system*

Despite the fact that a 2D corner is represented by four degrees of freedom, the sensor system is only allowed the **three** degrees of freedom, which are (referring to Figure I-8):

(i) the range,
(ii) the rotation $\alpha$ about $u$ axis and
(iii) the rotation $\beta$ about $v$ axis.

The purpose of this restriction is to reduce the mathematical complexity involved in the geometrical analysis of reflections from a 2D corner. The restriction on the allowable degrees of freedom of the sensor system does not affect the identification and location of planes and 3D corners since both planes and vertices of 3D corners are defined by three parameters. It also does not affect the classification and location of 2D corners in indoor robot localisation problems as these corners are further restricted as described in the next section.

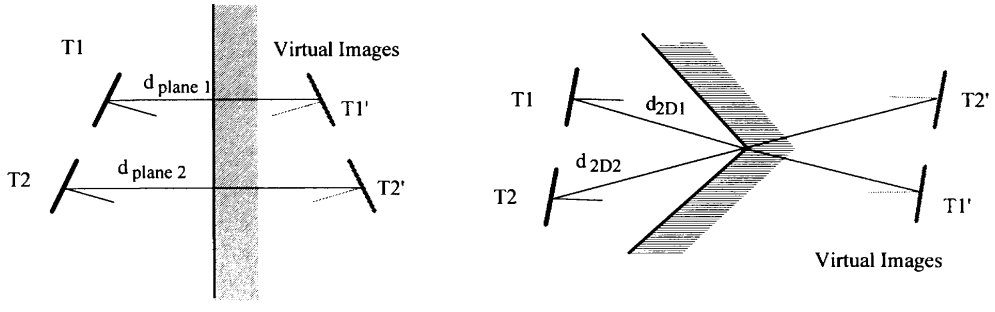


Fig. I-3. Projected views of a two-transducer system to illustrate the positions of the virtual images when the reflectors are a plane and a 2D corner.

https://doi.org/10.1017/S0263574797000581 Published online by Cambridge University Press

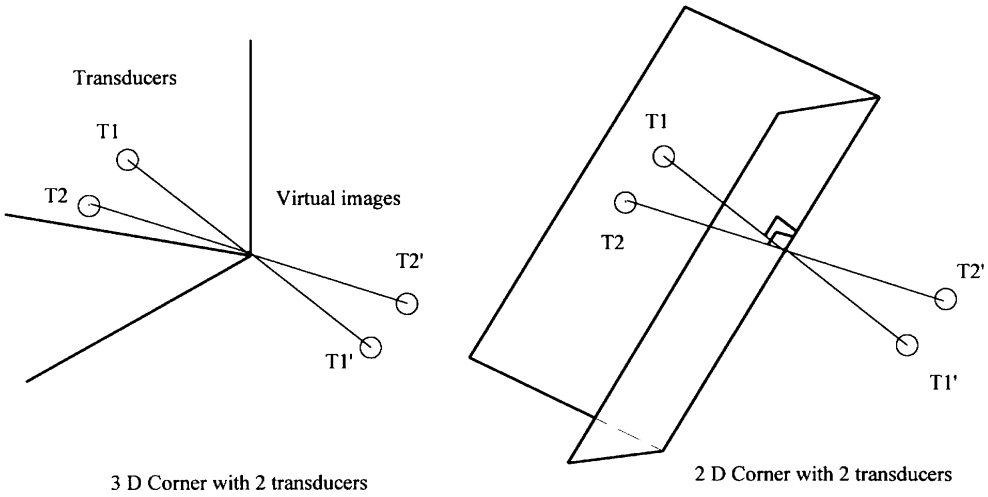


Fig. I-4. Virtual images of two transducers over a 3D corner and a possible 2D corner. Note that there is no difference in the location of the virtual images in the two cases.

## 5. V TERMS AND CONVENTIONS

*(a) Reflector classes*

The reflector class of 2D corner is subdivided into *2D Type I* and *2D Type II corners* which are illustrated in Figure I-8. The three allowable degrees of freedom of the sensor are sufficient for the purpose of robot localisation in an indoor environment since the ceiling-wall (floor-wall) and wall-wall intersections fall into one of the 2D corner categories, depending on the mounting of the triangular sensor system. There are thus *four* reflector classes which can be identified and located using this method.

*(b) Use of virtual images*

Although the transducers operate as both transmitters and receivers, it is easier to analyse the angular and distance relationships between signal paths if virtual images of transducers are used. The distance travelled by an echo from a transmitter to a receiver is thus equal to the length of the straight line joining the positions of the virtual transmitter and the receiver.

*(c) Choice of projection planes*

The simplification using virtual images described above still presents an unwieldly nest of lines in each reflector class. The problem can be further simplified if the 3D situation is projected onto appropriate 2D planes.

In the case of a plane target, the projection plane is chosen for two transducers at any one time such that both transducers and their respective virtual images lie on the projection surface. In the case of a 2D corner (Types I and II), two projections are required. It is observed that the unique path in a self-to-self reflection is perpendicular to the line of intersection formed by the two orthogonal planes of the corner. One projection plane is thus chosen to be perpendicular to this line of intersection. The other projection plane is orthogonal to the first projection plane but parallel to the normals of the transducers.

The virtual images of two transducers over a 3D corner and those over a suitably placed 2D corner are indistinguishable. Consequently, the 3D corner problem can be broken down into three 2D corner problems.

*(d) Choice of parameters and variables*

In the next Section, the geometrical relationships between the echo arrival times (or distances of flight) will be derived for the four reflector classes defined. It is thus necessary to define the conventions and the variables and parameters used.

- The inter-transducer spacing is $d$.
- The transducers are identified by $T1$, $T2$ and $T3$ and their virtual images $T1'$, $T2'$ and $T3'$ accordingly.

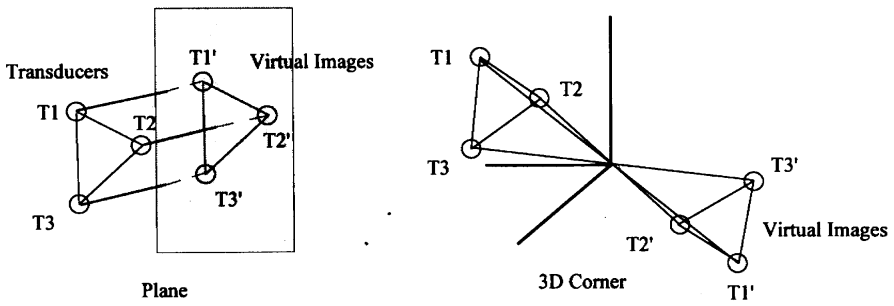


Fig. I-5. Virtual images of a three-transducer system over a plane and a 3D corner.

https://doi.org/10.1017/S0263574797000581 Published online by Cambridge University Press

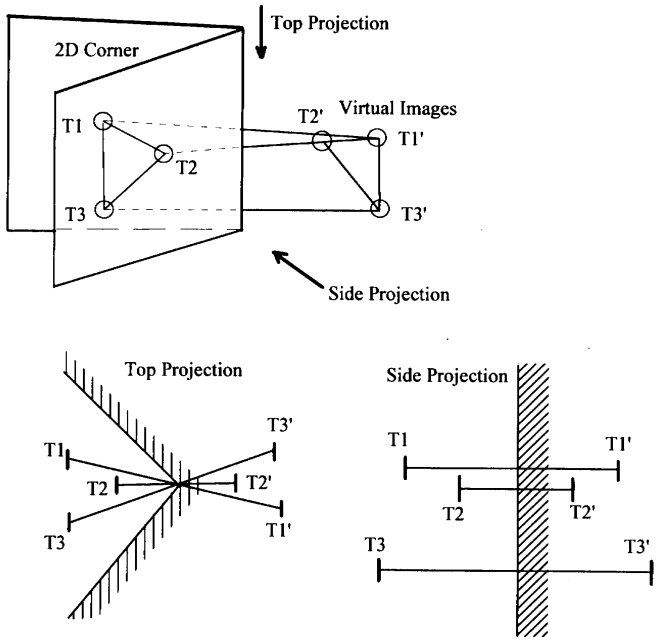


Fig. I-6. Virtual images of a three-transducer system over a 2D corner.

- Measurement of distance of flight is labelled $r_{ij}$ where $Ti$ is the transmitting transducer and $Tj$ is the receiving transducer. It is geometrically equivalent to the distance between the receiver and the virtual image of the transmitter.
- $r_{ij}$ and $r_{ji}$ are equal because the same path is taken in both directions (from transducer $i$ to transducer $j$ and vice versa).
- The convention for the signs of angles as seen in the 2D projections is negative if it is clockwise with respect to the normal (or its projection) of the transducer, positive if it is anticlockwise.
- The azimuth and elevation of an object with respect to the sensor coordinate frame are represented by $\alpha$ and $\beta$, the angles of rotation about $u$ and $v$ axes respectively.

## 6. GEOMETRICAL RELATIONSHIPS BETWEEN DISTANCES OF FLIGHT

In this section, all nine distances of flight $r_{ij}$ are expressed in terms of the three distances $r_{11}$, $r_{22}$, $r_{33}$, travelled by the

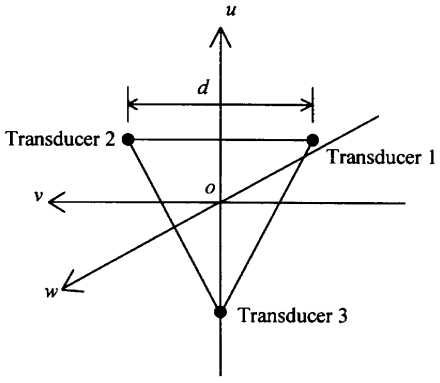


Fig. I-7. Triangular sensor arrangement.

Table I-1. 3D reflectors and the degrees of freedom of their representation in 3D space.

| 3D Landmark | Representation in 3D space | DOF |
|---|---|---|
| planes | planes | 3 |
| 2D corners | lines | 4 |
| 3D corners | points | 3 |

echoes from same transmitter to receiver for each reflector type. As will be shown later in this work, the three distances $r_{11}$, $r_{22}$, $r_{33}$, uniquely determine the position of the reflector for all the reflector types. From the relationships for $r_{ij}$, the Maximum Likelihood Estimation (MLE) technique will find the most likely estimates for $r_{11}$ $r_{22}$ $r_{33}$ and hence the *most likely location* of a matched object and also how well the nine $r_{ij}$ match the model. A good fit to the model is used to classify the reflector.

In this section, the mathematical derivations of the geometrical relationships are described. It is subdivided into the reflector classes: planes, 2D type I corner, 2D Type II corner and 3D corner.

*(a) Plane*

The transducers and their virtual images in the reflection off a plane are shown in Figure I-9. The following relationships are observed:

$$r_{22} = r_{11} + 2d \sin(\theta_{11}) \tag{I-1}$$

$$\theta_{11} = \theta_{22} \tag{I-2}$$

Note that $\theta_{11}$ and $\theta_{22}$ are positive according to the convention outlined in Section V. Using cosine rule on the triangle $T1$-$T2$-$T1'$ and equation (I-1):

$$r_{12}^2 = d^2 + r_{11}r_{22} \tag{I-3}$$

Projections similar to that shown in Figure I-9 can also be applied to transducer pairs $T2$ and $T3$, and $T3$ and $T1$ because the sensor system is symmetrical. The following relationships are obtained:

$$r_{23}^2 = r_{32}^2 = d^2 + r_{22}r_{33} \tag{I-4}$$

$$r_{31}^2 = r_{13}^2 = d^2 + r_{33}r_{11} \tag{I-5}$$

*(b) 2D type I corner*

The derivation for the 2D type I corner can be found in the Appendix at the end of this paper. The results are shown here:

$$r_{12} = r_{21} = \sqrt{\frac{r_{11}^2 + r_{22}^2}{2} - d^2} \tag{I-6}$$

$$r_{13} = r_{31} = \sqrt{\frac{d^2 + r_{11}^2 + r_{33}^2 - 3d^2\sin^2\rho}{2}} \tag{I-7}$$

$$r_{23} = r_{32} = \sqrt{\frac{d^2 + r_{22}^2 + r_{33}^2 - 3d^2\sin^2\rho}{2}} \tag{I-8}$$

https://doi.org/10.1017/S0263574797000581 Published online by Cambridge University Press

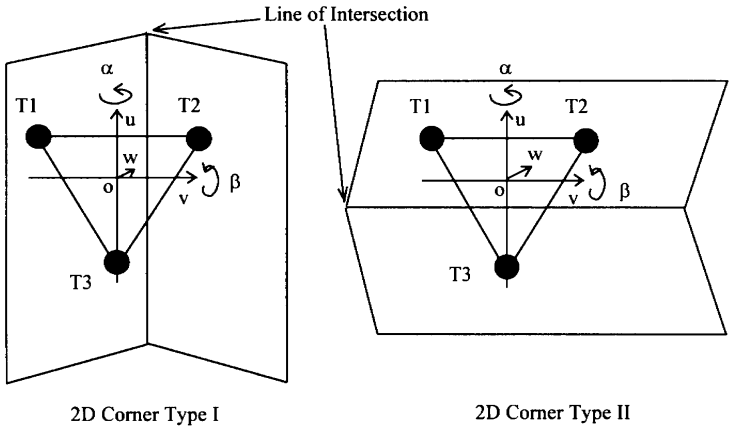


Fig. I-8. Type I and Type II 2D corners and the permitted axes ($u$ and $v$) of rotation. The origin of the coordinate frame lies on the centre of gravity of the equilateral triangular structure.

where $\sin\rho$ can be expressed in terms of $r_{11}$ $r_{22}$ $r_{33}$ using equations (I-35, I-33 and I-31).

*(c) 2D type II corner*

The signal paths taken by echoes between $T1$ and $T2$ are approximately parallel when the range distances $r_{11}/2$ and $r_{22}/2$ are large compared to the length $d\sin\rho$ where $\rho$ is the angle of azimuth. Ultrasonic transducers have a half-beamwidth angle $\theta_0$ where the transmitted pulse amplitude at angle $\theta_0$ to normal is 0.135 that of normal. If the sensor system is rotated about the $v$ axis by an angle larger than $\theta_0$, some of the echo signals received will be too small to be measured accurately on this sensor system. Therefore values of $\rho$ greater than $\theta_0$ will not produce a valid set of time-of-flight measurements. For the assumption of parallelism to be valid, it is necessary to verify that $d\sin\theta_0$ is small as compared to the minimum desirable range of operation.

This assumption of parallelism simplifies the derivation because it implies that the reflections between $T1$ and $T2$ over the 2D type II corner in Figure I-10 can be analysed like the reflections off a plane. This gives

$$r_{12} = r_{21} \cong \sqrt{d^2 + r_{11}r_{22}} \tag{I-9}$$

$$\sin\rho \cong \frac{r_{22} - r_{11}}{2d} \tag{I-10}$$

Analysing the relationship between the transducer pairs $T1$, $T3$ and $T2$, $T3$ results in

$$r_{13} = r_{31} \cong \sqrt{\frac{r_{33}^2 + r_{11}^2 - d^2 - (r_{22} - r_{11})^2/4}{2}} \tag{I-11}$$

$$r_{23} = r_{23} \cong \sqrt{\frac{r_{33}^2 + r_{22}^2 - d^2 - (r_{22} - r_{11})^2/4}{2}} \tag{I-12}$$

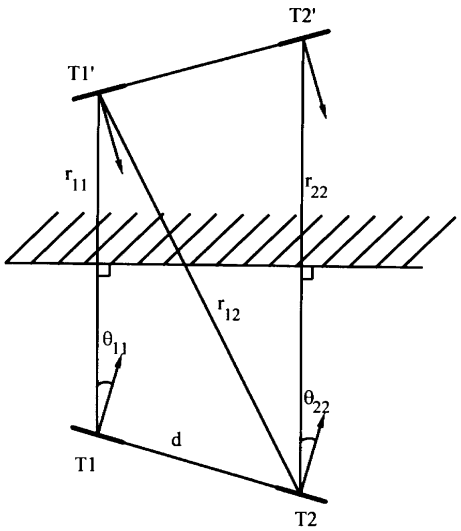


Fig. I-9. Illustration showing the virtual images and geometrical relationships between various distance of flight measurements for a plane.

*(d) 3D corner*

It has been shown in Section II that the virtual images of a two-transducer system over a 3D corner are the same as the same system positioned over a 2D Type I corner. This property can be exploited to facilitate the geometrical analysis of reflections off a 3D corner. If one pair of transducers is considered at a time, assuming the reflector is a 2D Type I corner, the following results are obtained:

$$r_{12} = r_{21} = \sqrt{\frac{r_{11}^2 + r_{22}^2}{2} - d^2} \tag{I-13}$$

$$r_{13} = r_{31} = \sqrt{\frac{r_{11}^2 + r_{33}^2}{2} - d^2} \tag{I-14}$$

$$r_{32} = r_{23} = \sqrt{\frac{r_{33}^2 + r_{22}^2}{2} - d^2} \tag{I-15}$$

## 7. MAXIMUM LIKELIHOOD ESTIMATION

During reflector identification, the Maximum Likelihood Estimator is employed to classify the reflector and to produce the *most likely* range parameters, $r_{11}$, $r_{22}$ and $r_{33}$,

https://doi.org/10.1017/S0263574797000581 Published online by Cambridge University Press

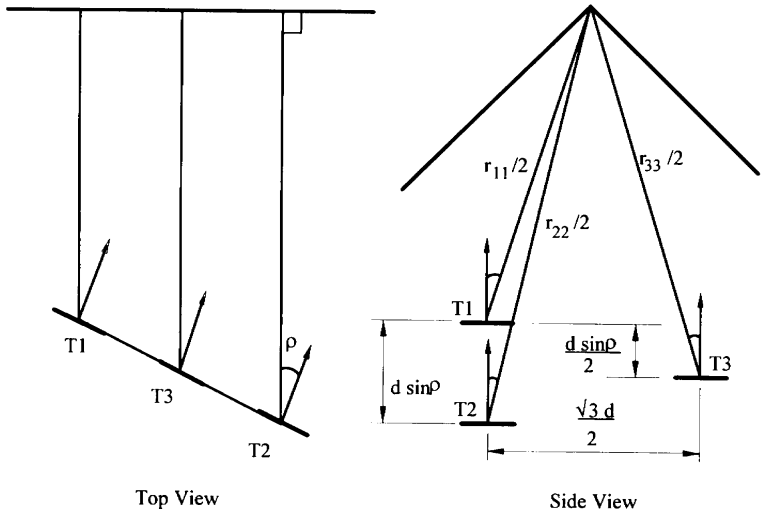


Fig. I-10. Illustration showing the geometrical relationships between the distances of flight corresponding to transducers $T1$, $T2$ and $T3$ for a 2D type II corner.

for its localisation. Equation (I-16) shows a $k$ dimension vector $\mathbf{Y}$ which is the sum of a $k$ dimensional vector $\mathbf{N}$ and a general function $F$ of an $i$ dimensional vector $\mathbf{X}$.

$$\mathbf{Y} = F(\mathbf{X}) + \mathbf{N} \tag{I-16}$$

$\mathbf{Y}$ can be viewed as a set of noisy measurements or observations of $F(\mathbf{X})$ where the noise contribution is represented by $\mathbf{N}$. The system is time invariant.

If the system is linear with Gaussian conditional proabability density functions and Gaussian noise with zero mean, the results of the MLE are easily obtained. Consider such a system with a $k$ dimensional observation vector $\mathbf{A}$, an $i$ dimensional parameter vector $\mathbf{B}$ and a $k$ dimensional Gaussian noise vector $\mathbf{N}$ with zero mean and covariance matrix $\mathbf{R}$. The linear relationship between $\mathbf{A}$ and $\mathbf{B}$ is expressed through a $k \times i$ matrix $\mathbf{J}$ as shown in equation (I-17),

$$\mathbf{A} = \mathbf{JB} + \mathbf{N} \tag{I-17}$$

the likelihood function is[18]

$$\Lambda(\mathbf{B}) = p[\mathbf{A} \mid \mathbf{B}] = \frac{1}{(2\pi)^{k/2}\,|\mathbf{R}|^{1/2}} \times \exp\{-\tfrac{1}{2}[(\mathbf{JB}-\mathbf{A})^{\mathrm{T}}\mathbf{R}^{-1}(\mathbf{JB}-\mathbf{A})]\} \tag{I-18}$$

The unbiased maximum likelihood estimate of $\mathbf{B}$, $\hat{\mathbf{B}}$, is obtained by maximising equation (I-18) and is:[18]

$$\hat{\mathbf{B}} = [\mathbf{J}^{\mathrm{T}}\mathbf{R}^{-1}\mathbf{J}]^{-1}\mathbf{J}^{\mathrm{T}}\mathbf{R}^{-1}\mathbf{A} \tag{I-19}$$

The scalar exponent in equation (I-18), reproduced in equation (I-20), is also called the least-squares error, $S$, which is minimised in the process of maximising $\Lambda(\mathbf{B})$.

$$S = (\mathbf{J}\hat{\mathbf{B}} - \mathbf{A})^{\mathrm{T}}\mathbf{R}^{-1}(\mathbf{J}\hat{\mathbf{B}} - \mathbf{A}) \tag{I-20}$$

This minimised value of $S$ is a measure of goodness of fit to the linear function in equation (I-17) and has a $\chi^2$ distribution with $k - i$ degrees of freedom.[19]

Based on the expressions for $r_{ij}$ derived in Section 6, equation (I-16) is set up in the following manner. The vector $\mathbf{Y}$ consists of the nine measurements labelled $m\_r_{ij}$ which correspond to the distances of flight between transmitter $i$ and receiver $j$. The parameter vector $\mathbf{X}$ contains the parameters $r_{11}$, $r_{22}$ and $r_{33}$. However, the function $F(\mathbf{X})$ in equation (I-16) is non-linear for all four reflector classes as is shown in Section 7. Linearisation is achieved using a Taylor expansion.

Linearisation of the function $F$ in equation (I-16) about $\mathbf{X_m}$, measured values $[m\_r_{11}, m\_r_{22}, m\_r_{33}]^{\mathrm{T}}$, gives

$$F(\mathbf{X}) - F(\mathbf{X_m}) \cong \mathbf{J}_{\mathbf{X_m}} \cdot [\mathbf{X} - \mathbf{X_m}] \tag{I-21}$$

where $\mathbf{J}_{\mathbf{X_m}}$ is the Jacobian of $F$ elaborated about $\mathbf{X_m}$. Equation (I-16) is rewritten as follows:

$$\begin{aligned}\mathbf{Y} - F(\mathbf{X_m}) &= F(\mathbf{X}) - F(\mathbf{X_m}) + \mathbf{N} \\ &\cong \mathbf{J}_{\mathbf{X_m}} \cdot [\mathbf{X} - \mathbf{X_m}] + \mathbf{N}\end{aligned} \tag{I-22}$$

which is the form of equation (I-17) with

$$\begin{aligned}\mathbf{A} &= \mathbf{Y} - F(\mathbf{X_m}) \\ \mathbf{B} &= \mathbf{X} - \mathbf{X_m} \\ \mathbf{J} &= \mathbf{J}_{\mathbf{X_m}}\end{aligned} \tag{I-23}$$

Vector $\mathbf{A}$ in equation (I-23) is thus constructed as shown below.

$$\mathbf{A} = \begin{bmatrix} 0 \\ 0 \\ 0 \\ m\_r_{12} - r_{12}(m\_r_{11}, m\_r_{22}, m\_r_{33}) \\ m\_r_{21} - r_{21}(m\_r_{11}, m\_r_{22}, m\_r_{33}) \\ m\_r_{13} - r_{13}(m\_r_{11}, m\_r_{22}, m\_r_{33}) \\ m\_r_{31} - r_{31}(m\_r_{11}, m\_r_{22}, m\_r_{33}) \\ m\_r_{23} - r_{23}(m\_r_{11}, m\_r_{22}, m\_r_{33}) \\ m\_r_{32} - r_{32}(m\_r_{11}, m\_r_{22}, m\_r_{33}) \end{bmatrix} = \mathbf{JB} + \mathbf{N} \tag{I–24}$$

The top nine entries in the $9 \times 3$ Jacobian matrix $\mathbf{J}$ resembles the $3 \times 3$ identity matrix as the range measurements $r_{11}$, $r_{22}$ and $r_{33}$ are deemed to be

https://doi.org/10.1017/S0263574797000581 Published online by Cambridge University Press

independent. The functions $r_{ij}(r_{11}, r_{22}, r_{33})$ have been derived in Section 6. The random Gaussian noise matrix $N$ has zero mean and covariance $\mathbf{R}$. The most likely estimate of $\mathbf{B}$, $\hat{\mathbf{B}}$, is evaluated using equation (I-19).

$$\mathbf{J} = \begin{bmatrix} 1 & 0 & 0 \\ 0 & 1 & 0 \\ 0 & 0 & 1 \\ \frac{\partial r_{12}}{\partial r_{11}} & \frac{\partial r_{12}}{\partial r_{22}} & \frac{\partial r_{12}}{\partial r_{33}} \\ \vdots & \vdots & \vdots \\ \frac{\partial r_{32}}{\partial r_{11}} & \frac{\partial r_{32}}{\partial r_{22}} & \frac{\partial r_{32}}{\partial r_{33}} \end{bmatrix}, \quad \hat{\mathbf{B}} = \begin{bmatrix} \hat{r}_{11} - m\_r_{11} \\ \hat{r}_{22} - m\_r_{22} \\ \hat{r}_{33} - m\_r_{33} \end{bmatrix} \tag{I-25}$$

Four values of $S$ corresponding to the four classes of reflectors are obtained with the nine measurements and equation (I-20). Each of these is a measure of the goodness of fit of the measured distances of flight to one of the reflector models and has a $\chi^2$ distribution with six (nine observations – three parameters) degrees of freedom. It is obvious that the least-squares error corresponding to the wrong reflector class will be much larger than that for the right reflector class. The $\chi^2$ table can be used for decision making. A fit is considered "acceptable" if

$$P\{S > c\} = \varepsilon \tag{I-26}$$

or equivalently,

$$P\{S \leq c\} = 1 - \varepsilon \tag{I-27}$$

where the threshold $c$ is obtained from the tables such that the probability of $S$ exceeding $c$ is $\varepsilon$ (usually 5% or 10%).[19] From the $\chi^2$ distribution with six degrees of freedom, the value corresponding to an $\varepsilon$ of 5% is 12.6.

The categorisation algorithm is therefore:

**"If an $S$ value is equal to or less than $c$, the test object is considered to belong to that reflector class. A test object cannot be categorised if all four $S$ values exceed $c$, or if the observations fit more than one of the reflector classes."**

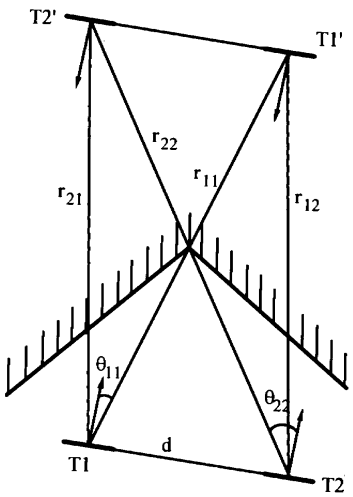


Fig. I-11. Illustration showing the virtual images and geometrical relationships between various distance of flight measurements of transducers $T1$ and $T2$ for a 2D Type I corner.

## CONCLUDING REMARKS

This concludes the first part of this work. The theory for the classification of 3D room features using the Maximum Likelihood Estimation using the ultrasonic sensor has been presented. The derivation of the localisation of objects in 3D space, together with the experimental results of this MLE technique on static objects and in a robot localisation problem, will be published in the next issue of *Robotica.* All references are located there at the end of Part II.

## APPENDIX: DERIVATION OF 2D TYPE I CORNER GEOMETRICAL RELATIONSHIPS

Consider the transducers $T1$ and $T2$ initially. Using the angle sign convention stated in Section 5, $\theta_{11}$ in Figure I-11 is negative while $\theta_{22}$ is positive. It can be seen that from triangles $T1$-$T2$-$T2'$ and $T1$-$T2$-$T1'$,

$$r_{22} \sin \theta_{22} - r_{11} \sin \theta_{11} = 2d \tag{I-28}$$

$$r_{22} \cos \theta_{22} = r_{11} \cos \theta_{11} \tag{I-29}$$

Using the cosine rule on the two above triangles, it is found that

$$r_{12} = r_{21} = \sqrt{\frac{r_{11}^2 + r_{22}^2}{2} - d^2} \tag{I-30}$$

The following results are also obtained.

$$\theta_{11} = \sin^{-1}\left(\frac{r_{22}^2 - r_{11}^2 - 4d^2}{4 r_{11} d}\right) \tag{I-31}$$

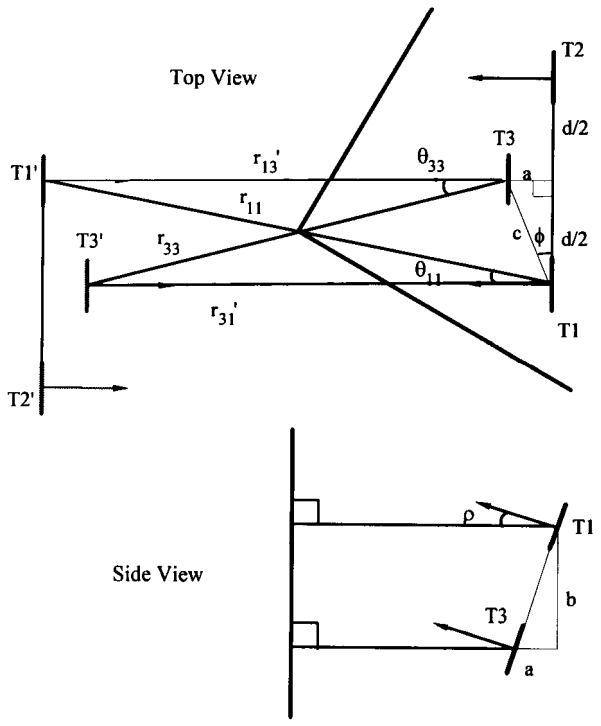


Fig. I-12. Illustration showing both top and elevation views of the virtual images of transducers $T1$, $T2$ and $T3$ over a 2D Type I corner.

https://doi.org/10.1017/S0263574797000581 Published online by Cambridge University Press

Consider a rotation of angle $\rho$ about $v$ axis which has resulted in the position of transducer $T3$ with respect to $T1$ and $T2$ as shown in Figure I-12. The top view illustrated in Figure I-12 is similar to that shown in Figure I-11 with the major difference being the inclusion of transducer $T3$.

Using the same method of derivation for equation (I-28),

$$r_{33}\sin\theta_{33} - r_{11}\sin\theta_{11} = 2d \tag{I-32}$$

Substituting $\theta_{11}$ in the above equation results in:

$$\theta_{33} = \sin^{-1}\left(\frac{r_{22}^2 - r_{11}^2}{4dr_{33}}\right) \tag{I-33}$$

Similarly, using the same method of derivation for equation (I–29),

$$r_{11}\cos\theta_{11} - r_{33}\cos\theta_{33} = \sqrt{3}d\sin\rho \tag{I-34}$$

A change of variable produces

$$\rho = \sin^{-1}\left(\frac{r_{11}\cos\theta_{11} - r_{33}\cos\theta_{33}}{\sqrt{3}d}\right) \tag{I-35}$$

The values of $\sin\phi$, $\cos\phi$, $a$, $b$ and $c$ in Figure I-12 are:

$$\begin{aligned} \sin\phi &= \frac{a}{c}, \quad \cos\phi = \frac{d}{2c}, \\ a &= \frac{\sqrt{3}}{2}d\sin\rho, \\ b &= \frac{\sqrt{3}}{2}d\cos\rho, \\ c^2 &= a^2 + \frac{d^2}{4}. \end{aligned} \tag{I-36}$$

Using cosine rule again on the triangle formed by $T1$, $T3$ and $T1'$ and noting the angle convention for $\theta_{11}$:

$$\begin{aligned} r_{13}'^2 &= r_{11}^2 + c^2 - 2cr_{11}\cos\left(\frac{\pi}{2} + \theta_{11} - \phi\right) \\ &= r_{11}^2 + a^2 + \frac{d^2}{4} - 2ar_{11}\cos\theta_{11} + dr_{11}\sin\theta_{11} \end{aligned} \tag{I-37}$$

Similarly for the triangle formed by $T1$, $T3$ and $T3'$:

$$r_{31}'^2 = r_{33}^2 + a^2 + \frac{d^2}{4} + 2ar_{33}\cos\theta_{33} - dr_{33}\sin\theta_{33} \tag{I-38}$$

However, $r_{13}'$ and $r_{31}'$ are the projected lengths of $r_{13}$ and $r_{31}$ respectively. It is necessary to include the projection height, $b$, to obtain $r_{13}$ and $r_{31}$:

$$\begin{aligned} r_{13}^2 &= r_{13}'^2 + b^2 \\ &= r_{11}^2 + d^2 + r_{11}d\sin\theta_{11} - \sqrt{3}dr_{11}\sin\rho\cos\theta_{11} \end{aligned} \tag{I-39}$$

$$r_{31}^2 = r_{33}^2 + d^2 - r_{33}d\sin\theta_{33} + \sqrt{3}dr_{33}\sin\rho\cos\theta_{33} \tag{I-40}$$

Bearing in mind $r_{13} = r_{31}$,

$$r_{13} = r_{31} = \sqrt{\frac{d^2 + r_{11}^2 + r_{33}^2 - 3d^2\sin^2\rho}{2}} \tag{I-41}$$

Repeating the above process for triangles $T2$-$T3$-$T3'$ and $T2$-$T3$-$T2'$ arrives at

$$r_{23} = r_{32} = \sqrt{\frac{d^2 + r_{22}^2 + r_{33}^2 - 3d^2\sin^2\rho}{2}} \tag{I-42}$$

https://doi.org/10.1017/S0263574797000581 Published online by Cambridge University Press